JOURNAL OF BACTERIOLOGY, Nov. 1990, p. 6589–6595
0021-9193/90/116589--0$02.00/0

Vol. 172, No. 11

High-Resolution Topography of the S-Layer Sheath of the Archaebacterium *Methanospirillum hungatei* Provided by Scanning Tunneling Microscopy

T. J. BEVERIDGE,[1]* G. SOUTHAM,[1] M. H. JERICHO,[2] AND B. L. BLACKFORD[2]

Department of Microbiology, College of Biological Science, University of Guelph, Guelph, Ontario, N1G 2W1,[1] and Department of Physics, Dalhousie University, Halifax, Nova Scotia, B3J 2X4,[2] Canada

Received 8 June 1990/Accepted 21 August 1990

The inner and outer surfaces of the sheath of *Methanospirillum hungatei* GP1 have been imaged for the first time by using a bimorph scanning tunneling microscope (STM) on platinum-coated or uncoated specimens to a nominal resolution in height of ca. 0.4. nm. Unlike more usual types of microscopy (e.g., transmission electron microscopy), STM provided high-resolution topography of the surfaces, giving good depth detail which confirmed the sheath to be a paracrystalline structure possessing minute pores and therefore impervious to solutes possessing a hydrated radius of >0.3 nm. STM also confirmed that the sheath consisted of a series of stacked hoops ~2.5 nm wide which were the remnants of the sheath after treatment with 2% (wt/vol) sodium dodecyl sulfate–2% (vol/vol) β-mercaptoethanol (pH 9.0). No topographical infrastructure could be seen on the sides of the hoops. This research required the development of a new long-range STM capable of detecting small particles such as bacteria on graphite surfaces as well as a new "hopping" STM mode which did not deform the poorly conducting bacterial surface during high-resolution topographical analysis.

Spectacular images which accurately depict the lattice arrangement of surface atoms have been achieved by using the scanning tunneling microscope (STM) on surfaces of inert materials, such as thin metal foils and minerals (5, 6, 11). These images rely on the fact that when an extremely sharp probe such as a tungsten tip is brought to within a few angstroms of the specimen surface, a tunneling current is established which can accurately be monitored by the microscopist (5, 6, 11). The magnitude of the tunneling current is directly determined by the distance between microscope tip and specimen, and this phenomenon can be used for imaging. Usually the microscope tip is rastered across the specimen surface so that this current is kept constant. The tip, along its linear path over the specimen, is raised and lowered mechanically by piezoceramic devices to maintain a constant tunneling current, and consequently the topography of the specimen's contours along the tip's linear track can be recorded. With certain inert samples, this is so precise that atomic structure is revealed (5, 6, 11). Typically the raster pattern of the tip is over an area of 10 by 10 nm, and this is the usual size of the image.

Recently, there has been a surge of research on the use of STM on biological structures. Although surface structures of several organic molecules (10, 13) and biological structures (1, 2, 7–9) have been produced, it is apparent that these more deformable surfaces present special problems for high-resolution STM. For example, biological material often possesses poor electrical conductivity and acts as an insulator towards tunneling current; it is usually weakly bonded, soft, and easily deformable, and the chemical bonding between the biological specimen and the supporting STM substratum is noncovalent and easily broken. In addition for microbiology, bacterial cells and their components are extremely small and when spread over an STM support surface, such as graphite, are extremely difficult to find by an STM with a rastering area of ca. 10 by 10 nm.

The surface structure of the archaebacterial methanogen *Methanospirillum hungatei* is a sheath (Fig. 1) which consists of a series of proteinaceous hoops (see Fig. 4) attached to one another to form a hollow cylinder in which chains of cells reside, separated from each other by "cell spacers" (3, 18). A model of the sheath showing its structure and some chemical bonding can be found in Fig. 8 of reference 15. Studies using chemical denaturants have shown that the sheath is extremely insensitive to degradation and suggest that most bonding between constituent polymers is covalent (4). Although the sheath has been well studied by conventional transmission electron microscopy and a high-resolution structure has been described (14, 17), the unit cell of its paracrystalline lattice is so small that accurate topographical analysis has been impossible except by contour plots generated by computer analysis (17). The description of the sheath as an S layer consisting of small (2.8-nm) particles surrounded by similar-sized pores (14, 17) is more intuitive than factual and is based on electron density patterns generated by heavy metal negative stains. Yet, these same studies have provided a precise model and in fact have predicted the secondary polypeptide structure (cross-beta) of the subunits (17). A new topographical method was necessary to provide accurate contour and depth analysis for comparison with the transmission electron microscopy models. The two characteristics of the sheath, high covalent bonding and a precise macromolecular surface lattice, made this structure an ideal bacterial surface to attempt, for the first time in microbiology, to image by STM; it would be a suitable biological object to test the resolution of this new microscopical technique. In addition, because the sheath can be readily broken up by chemical means into even smaller (but structurally distinct) hoops, we could test the capability of the bimorph STM (6) to find and discriminate such minute objects as hoops from the background of the graphitic support surface.

* Corresponding author.

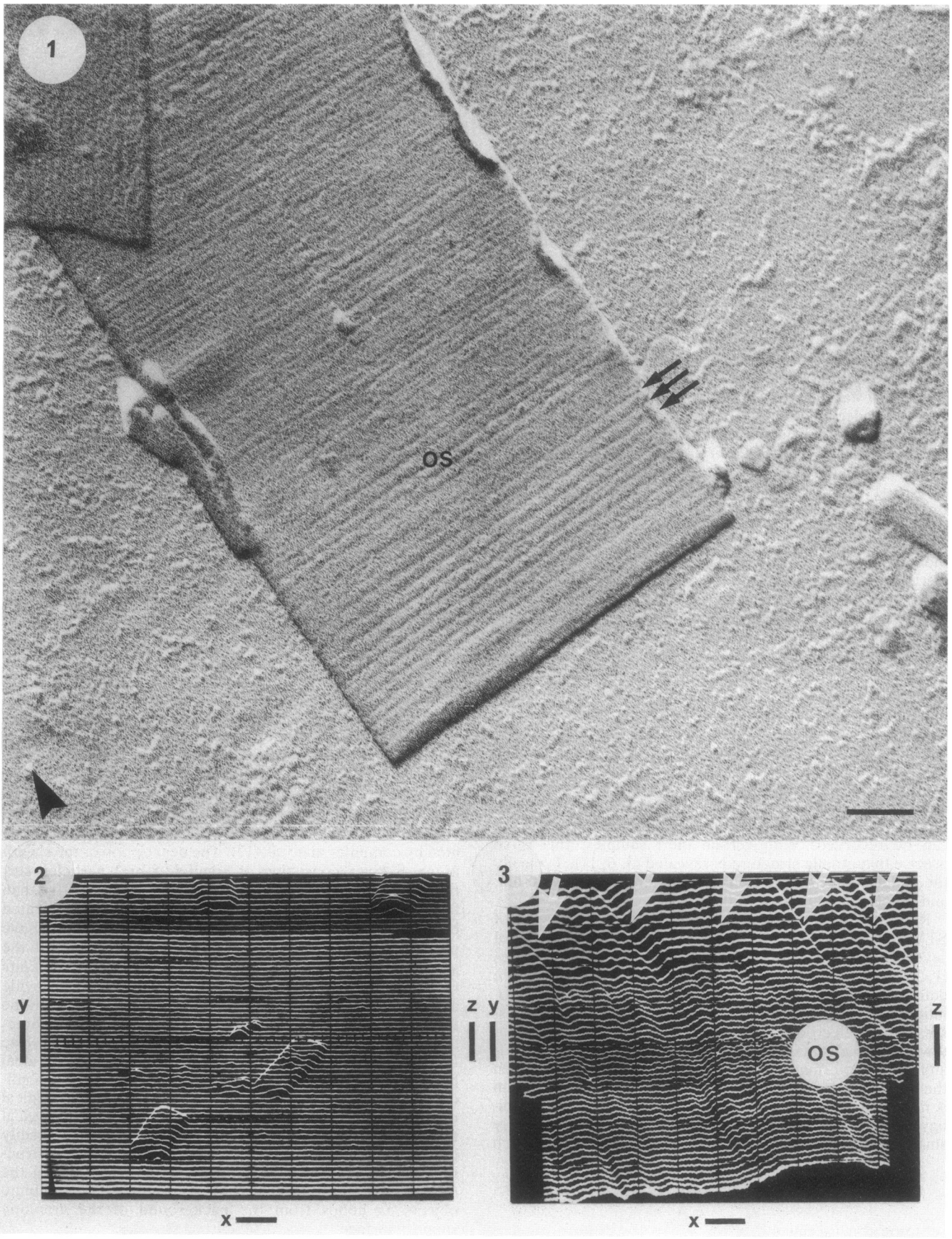

M. hungatei GP1 sheaths were isolated from growing cultures as described by Sprott et al. (16), and the spacer plugs were removed by brief treatment with 0.1 N NaOH (15, 17). Before STM imaging, the sheaths were dialyzed extensively in deionized and distilled water. A drop of a relatively dilute suspension (OD_{600}, 0.10) was placed on a freshly cleaved, single-crystal graphite surface to allow the sheaths to sorb from suspension. After 2 min the drop was removed and the graphite surface was allowed to air dry. In some experiments, a 2.5- to 5.0-nm Pt or C coating was deposited over the entire surface (sample plus graphite) to increase conductivity before STM imaging. Electron microscopy of the suspensions prior to STM ensured that the sheath's lattice was intact and that each cylindrical fragment was ca. 0.5 μm in diameter and 1.0 to 5.0 μm in length.

The STM is based on the piezoelectric bimorph design of Blackford et al. (6). The 25-mm-diameter bimorph elements of the STM produced a scan range of 8.0 by 8.0 μm, which provided large raster areas suitable for detecting individual sheath fragments (Fig. 2), yet the STM was still capable of atomic resolution images of graphite (6). All STM images shown in Fig. 2, 3, and 5 were obtained by using the constant-tunneling-current mode. The large scanning range of our STM resulted in low-resonance frequencies (~500 Hz) of mechanical movement, and slow scanning speeds were required for imaging. Typically speeds of 0.1 to 0.5 μm/s were used for long-range imaging (Fig. 2). The *Y* signal was the sum of the *y* raster voltage and the *z* piezo feedback voltage. All STM images are unprocessed and represent the raw data from each scan. The tunneling current was 0.1 nA, and the tip bias was −1.0 V.

Platinum-coated specimens. High-resolution scans of the surface of one Pt-coated sheath revealed row structures aligned at right angles to the sheath cylinder axis (Fig. 3) and with widths in multiples of a 3.0-nm minimum period (see also reference 7). These topographical features are expected for a crystalline surface composed of 2.8-nm particles (17) which has been coated with 2.5 to 5.0 nm of Pt, and they correspond well with features of the outer surface of the sheath which had been shadowed with Pt for transmission electron microscopy (Fig. 1).

However, because these Pt-STM images are of metal-coated specimens, it is difficult to entirely reconcile them directly with the high-resolution transmission electron microscope images of negatively stained material obtained by Stewart et al. (17). Even though high-resolution images of the outer surface which show the 2.8-nm particles of the S-layer lattice have been produced by this method (Fig. 4 in reference 7), the metal coating may not exactly mimic the arrangement of the particles and the metal will have its own inherent granularity.

Smaller test object and carbon coating. To further test the discriminating power of our STM, we decided to chemically disassemble the sheaths, by treatment in 2% (wt/vol) sodium dodecyl sulfate–2% (vol/vol) β-mercaptoethanol (pH 9.0) at 90°C for 30 min (15), into their hoops, which were at least 50 times smaller in length than the sheath. Of additional interest was to see if the sides of the sheath possessed discernible infrastructure, since it was in these regions that chemical bonds had been broken by the disruptive agents. Electron microscopy showed the hoops to lie flat on the support surface so that the 2.8-nm particles lay on the outside periphery (Fig. 4). This time, so as not to detract so much from the native surface features with metal aggregates, Pt was not used as a coating to increase conductivity. Instead, a thin coating of carbon was used; this increases conductivity but uses an atom smaller than Pt and does not form aggregates on the chemically charged sites of the specimen. As in the former case, the sheath material (i.e., hoops) was readily detected by the long-range scanning mode of the STM and could easily be discerned from the support surface even though the hoops were much smaller than the complete sheath (Fig. 5). Infrastructure was not evident on the sides of the hoops. For these samples, when the imaging (tunneling) current and/or bias (tip) voltage was increased, the structures deformed. It was apparent that C coating was not as conductive as Pt coating for STM tunneling currents.

Use of hopping-mode STM. The previous experiments had shown that even with strongly bonded biological surfaces, such as the sheath of *M. hungatei*, the currents established between STM tip and sample could be so strong that deformation and collapse of native structure were frequent. Metal coatings can preserve structure because of their good conductivity, but their depositional granularity detracts from use for extremely high resolutions. Carbon coatings are not as granular, but they are also not as conductive for the higher tunneling currents required during high resolution. Yet, the inescapable conclusion is that if STM imaging of samples is to be of major consequence in biology, high resolution of native uncoated surfaces will be required.

FIG. 1. Transmission electron micrograph of a platinum-shadowed collapsed sheath of *M. hungatei*, showing the wave pattern of hoops or hoop lines (arrows) in the outer surface (OS). The arrowhead denotes the shadow direction. Bar, 100 nm.

FIG. 2. STM image of sheath spread over a graphite surface, using the long-range scanning mode and 2.5-nm platinum coating. Two complete sheaths can be seen in the middle of this image. Bars: *x* and *y*, 0.6 μm; *z*, 0.12 μm.

FIG. 3. High-resolution STM image of the Pt-coated outer surface (OS) of a sheath. The OS has been identified as such by the narrow continuous valleys (arrows) along its surface; these valleys represent the hoop lines (i.e., where each hoop is attached; see Fig. 6). Since the STM scan lines approach the dimensions of the subunit particles, they cannot be seen. Bars: *x* and *y*, 12 nm; *z*, 6 nm.

FIG. 4. Transmission electron micrograph of negatively stained (1% uranyl acetate) hoops, showing the 2.8-nm particle distribution at the periphery of the outer surface. Bar, 100 nm.

FIG. 5. STM image of a carbon-coated preparation similar to that seen in Fig. 4. Bars: *x* and *y*, 120 nm; *z*, 40 nm.

FIG. 6. Transmission electron micrograph of a platinum-shadowed French pressure cell-sheared *M. hungatei* sheath fragment. Because the fragment is twisted, both the outer surface (OS) and the inner surface (IS) are visible. Hoop lines are visible on each surface (arrows). The arrowhead denotes the shadow direction. Bar, 100 nm.

FIG. 7. Intermediate magnification of an uncoated French-pressed sheath fragment, using the hopping mode. The broad striations or continuous hills (arrows) on the fragment which are at right angles to the scans are the hoop lines and reveal this to be the inner surface (IS) (see Fig. 6). Bars: *x* and *y*, 30 nm; *z*, 8 nm.

FIG. 8. Extremely high-resolution STM image of the surface of the uncoated sample in Fig. 7, using the hopping mode. Bars: *x* and *y*, 3 nm; *z*, 0.4 nm. Resolution in the *z* direction is at least 0.4 nm.

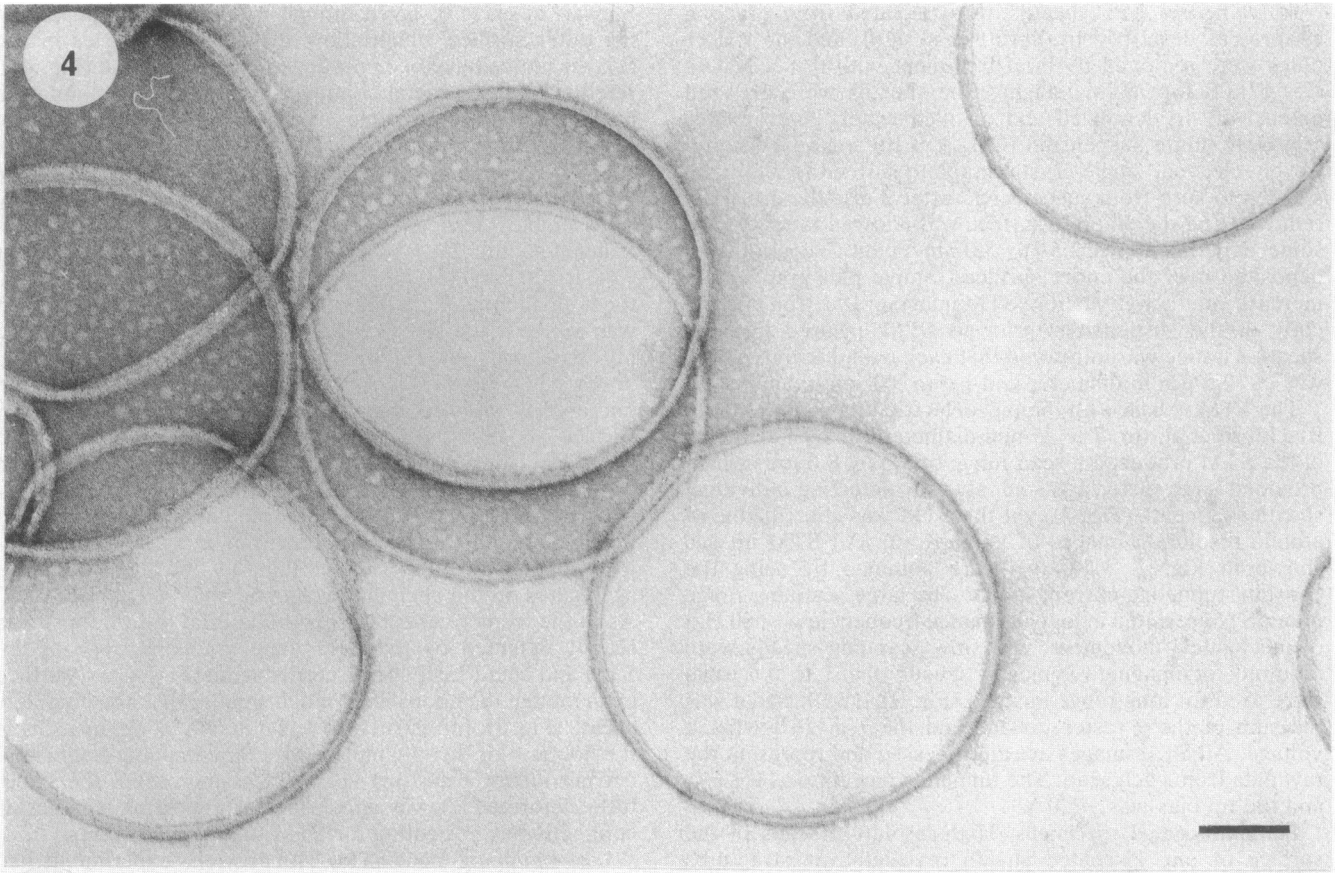

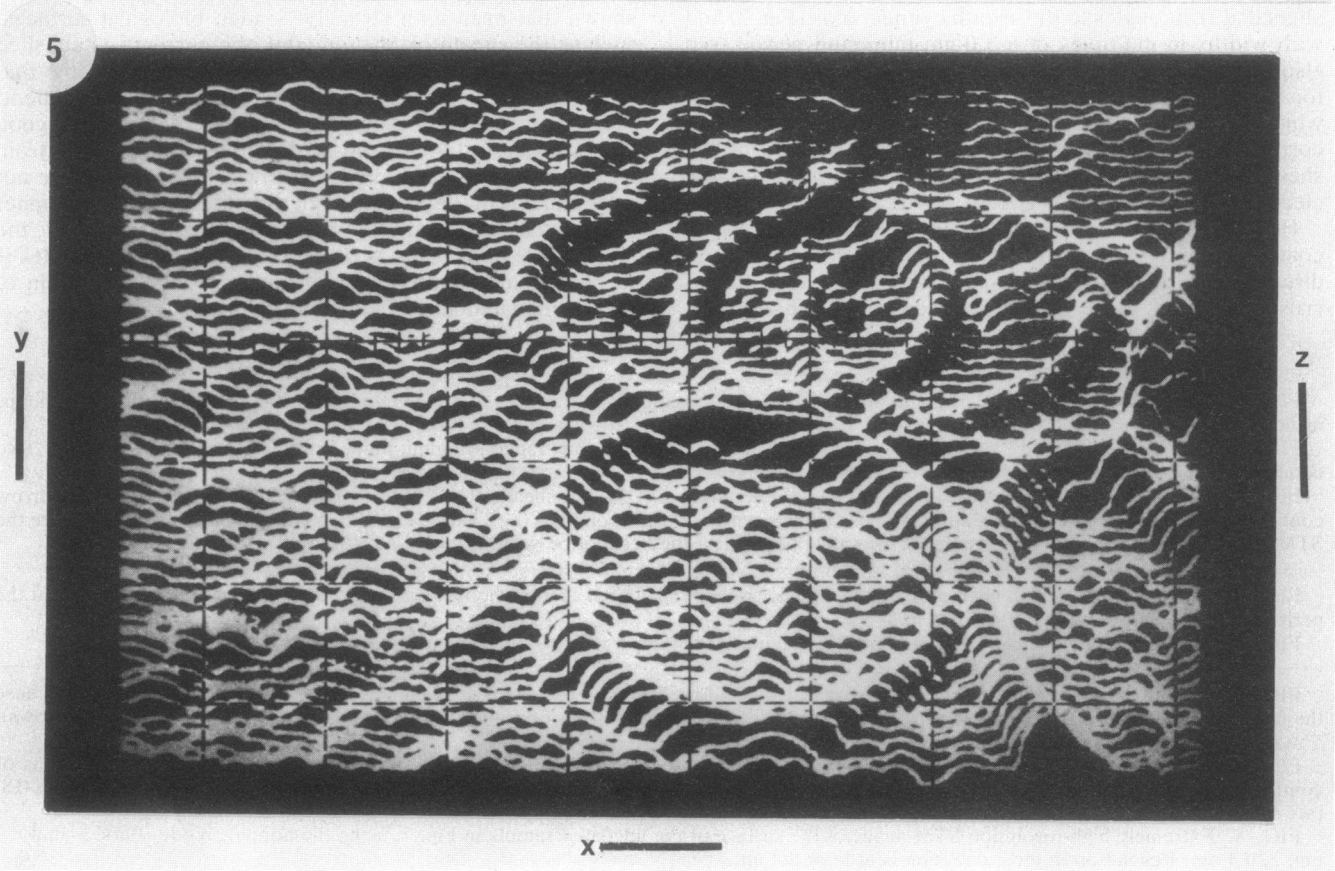

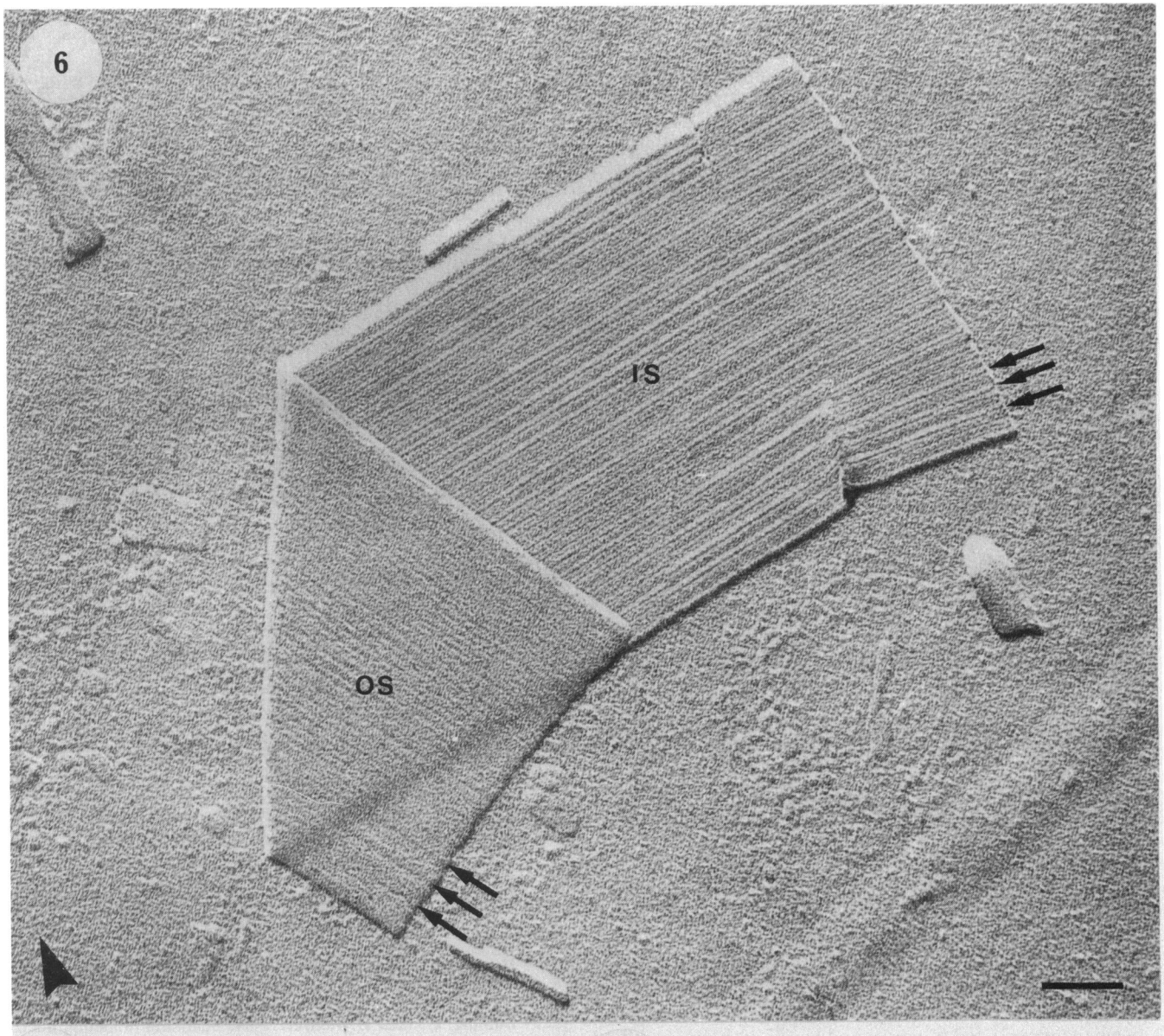

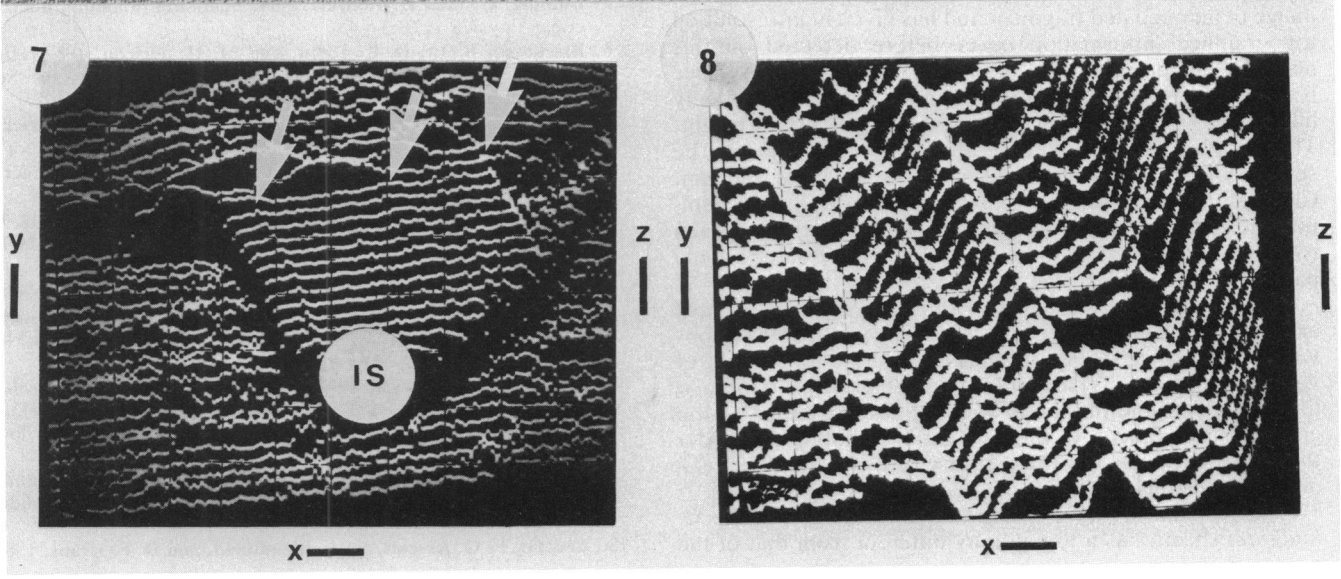

In the usual operating mode, the STM tip is continually scanned across the specimen surface and tip-to-specimen interactions are strong. Enough lateral stress builds up to deform native structure or even to entirely dislodge the specimen from its support surface. These are stresses which require time to build and to impose an effect. In order to minimize these effects an entirely new scanning mode was developed, in which the STM tip is frequently pulled back from the surface and tunneling is interrupted. While the tip is raised it is moved a short distance along the surface before a new approach is made; it is "hopped" along the surface, and a simple analogy is the movement of a sewing machine needle as it stitches along a cloth. The complete hopping process is monitored with the detection of the rise and fall of the tunneling current, and the z piezo voltage is detected by a boxcar integrator whose output is added to the y raster voltage to be displayed in the usual way (12). The time elapsed between raising and lowering the tip, is typically on the order of 5 to 6 ms. Because it was noticed that whole intact sheath flattened and compressed against the support surface on drying (Fig. 2), we decided to physically break up sheaths into smaller flat and less deformable fragments by passing them three times through a French pressure cell at 18,000 lb/in^2. This produced fragments of 100 to 150 nm by 150 to 500 nm which attached to the support surface by either the sheath's outer or inner surface (see Fig. 6 for orientation). Select area electron diffraction using a Philips EM400T revealed 2.8-nm reflections, which suggested that the fragments had not deformed during drying. Uncoated preparations of this French-pressed material were used for hopping-mode STM. Since the outer surface had previously been shown at high resolution by Blackford et al. (7) and the 2.8-nm subunit particles had been imaged, we concentrated on the inner surface using the hopping mode.

The small sheath fragments were first located by using the normal long-range scanning mode. Intermediate magnifications using the hopping mode made surface identification possible, and small regions of the identified surface could then be scanned at extremely high resolution in the hopping mode. For example, Fig. 7 shows the inner surface of a fragment (identified as such by the broad striations on its surface at right angles to the scan direction) at an intermediate magnification, whereas Fig. 8 is a high-resolution image of a small portion of the fragment. The hopping mode has produced at least 0.4-nm resolution along the z axis in this image of an uncoated fragment and has given high-resolution topographical information never before detected on this normally hidden surface (cf. Fig. 1, 6, and 8). The flat surface between the broad grooves on the inner surface are actually filled with ~3.0-nm rows that are 0.4 to 0.7 nm in height. These rows can follow one after the other or can be separated by a relatively flat interval of about 6.0 nm. Clearly, this inner-surface topography is not entirely reminiscent of that of the outer surface, although the ~3.0-nm row lines are similar to those produced by the outer 2.8-nm particles (Fig. 3; 17).

We suggest that these broad intervals running at right angles to the sheath's long axis denote the width of the hoops which are stacked together. Since STM shows them to be of variable width (Fig. 7) and since they all show ~3.0-nm row lines, it is possible that hoop width is associated with hoop growth and maturity. In this context broad hoops are older than narrow hoops and the capacity of hoops to widen is a necessity for the growth of the filament.

In conclusion, we have shown that the inner face of the *M. hungatei* sheath has a topography different from that of the outer face when the high-resolution features are compared (14, 17). Yet, the ~3.0-nm row lines of the inner aspect are analogous to the 2.8-nm subunit repeat and suggest that the unit cell is preserved on both surfaces. The low regions seen by STM on the inner surface (Fig. 7) provide additional support for continuous holes, or pores, through the sheath, since they have also been seen in STM images of the outer surface (7), in contour plots (17), and in hoop profiles (17).

We have shown that there can be great benefits from the application of STM to elucidate bacterial surface topography to high resolution. Coated surfaces, using Pt or C, are suitable for the intermediate magnifications required to image intact sheaths (Fig. 2 and 3) or hoops (Fig. 5), but the tip currents required for higher magnifications can deform high-resolution structure. A new "hopping" STM mode was needed for extremely high magnification of uncoated surfaces (Fig. 8). It is impossible at this time to know the resolution limits of the hopping mode on biological surfaces. Clearly, as shown by this report, submolecular resolution is possible and, if a surface is well bonded and naturally conducting, atomic resolution may be achieved. We are currently striving for higher resolution. This new STM mode may be appropriate for the viewing of other, less robust bacterial surfaces such as murein sacculi, outer membranes, and other S layers.

This research was supported by a Medical Research Council of Canada (MRC) grant to T.J.B. Operating funds to T.J.B. from the MRC and to M.H.J. and B.L.B. from the Natural Sciences and Engineering Research Council of Canada (NSERC) allowed the STM to be designed, built, and modified. G.S. was the recipient of an NSERC Graduate Student Fellowship.

LITERATURE CITED

1. **Amrein, M., R. Dürr, A. Stasiak, H. Gross, and G. Travaglini.** 1989. Scanning tunneling microscopy of uncoated recA-DNA complexes. Science **243**:1708–1711.
2. **Amrein, M., A. Stasiak, H. Gross, E. Stroll, and G. Travaglini.** 1988. Scanning tunneling microscopy of recA-DNA complexes coated with a conducting film. Science **240**:514–516.
3. **Beveridge, T. J., B. J. Harris, and G. D. Sprott.** 1987. Septation and filament splitting in *Methanospirillum hungatei*. Can. J. Microbiol. **33**:725–732.
4. **Beveridge, T. J., M. Stewart, R. J. Doyle, and G. D. Sprott.** 1985. Unusual stability of the *Methanospirillum hungatei* sheath. J. Bacteriol. **162**:728–737.
5. **Binning, G., and H. Rohrer.** 1984. Scanning tunneling microscopy. Physica **127B**:37–45.
6. **Blackford, B. L., D. C. Dahn, and M. H. Jericho.** 1987. High stability bimorph scanning tunneling microscope. Rev. Sci. Instrum. **58**:1343–1348.
7. **Blackford, B. L., M. O. Watanabe, D. C. Dahn, M. H. Jericho, G. Southam, and T. J. Beveridge.** 1989. The imaging of a complete biological structure with the scanning tunneling microscope. Ultramicroscopy **27**:427–432.
8. **Blackford, B. L., M. O. Watanabe, M. H. Jericho, and D. C. Dahn.** 1988. STM imaging of the complete bacterial cell sheath of *Methanospirillum hungatei*. J. Microsc. **152**:237–243.
9. **Dahn, D. C., M. O. Watanabe, B. L. Blackford, M. H. Jericho, and T. J. Beveridge.** 1988. Scanning tunneling microscopy imaging of biological structures. J. Vac. Sci. Technol. **A6**:548–552.
10. **Foster, J. S., and J. E. Frommer.** 1988. Imaging of liquid crystals using a tunneling microscope. Nature (London) **333**:542–545.
11. **Golovichenko, J. A.** 1986. The tunneling microscope: a new look at the atomic world. Science **232**:48–53.
12. **Jericho, M. H., B. L. Blackford, and D. C. Dahn.** 1989. Scanning tunneling microscope imaging technique for weakly bonded surface deposits. J. Appl. Phys. **65**:5237–5239.
13. **Lee, G., P. G. Arscott, V. A. Bloomfield, and D. F. Evans.** 1989.

Scanning tunneling microscopy of nucleic acids. Science **244:** 475–477.
14. **Shaw, P. J., G. J. Hills, J. A. Henwood, J. E. Harris, and D. A. Archer.** 1985. Three-dimensional architecture of the cell sheath and septa of *Methanospirillum hungatei*. J. Bacteriol. **161:**750–757.
15. **Sprott, G. D., T. J. Beveridge, G. B. Patel, and G. Ferrante.** 1986. Sheath disassembly in *Methanospirillum hungatei* GP1. Can. J. Microbiol. **32:**847–854.
16. **Sprott, G. D., J. R. Calvin, and R. C. McKeller.** 1979. Spheroplasts of *Methanospirillum hungatei* formed upon treatment with dithiothrietol. Can. J. Microbiol. **25:**730–738.
17. **Stewart, M., T. J. Beveridge, and G. D. Sprott.** 1985. Crystalline order to high resolution in the sheath of *Methanospirillum hungatei*: a cross-beta structure. J. Mol. Biol. **183:**509–515.
18. **Zeikus, J. G., and V. G. Bowen.** 1975. Fine structure of *Methanospirillum hungatei*. J. Bacteriol. **121:**373–380.